Fast Stochastic Surrogate Modeling via Rational Polynomial Chaos Expansions and Principal Component Analysis

PAOLO MANFREDI[ID], (Senior Member, IEEE), AND STEFANO GRIVET-TALOCIA[ID], (Fellow, IEEE)

Department of Electronics and Telecommunications, Politecnico di Torino, 10129 Torino, Italy

Corresponding author: Paolo Manfredi (paolo.manfredi@polito.it)

ABSTRACT This paper introduces a fast stochastic surrogate modeling technique for the frequency-domain responses of linear and passive electrical and electromagnetic systems based on polynomial chaos expansion (PCE) and principal component analysis (PCA). A rational PCE model provides high accuracy, whereas the PCA allows compressing the model, leading to a reduced number of coefficients to estimate and thereby improving the overall training efficiency. Furthermore, the PCA compression is shown to provide additional accuracy improvements thanks to its intrinsic regularization properties. The effectiveness of the proposed method is illustrated by means of several application examples.

INDEX TERMS Multiport systems, polynomial chaos, principal component analysis, rational modeling, surrogate modeling, variability analysis, uncertainty quantification.

I. INTRODUCTION

Uncertainty quantification is becoming ubiquitous in many engineering domains. In fact, the intrinsic variability of many design parameters, such as geometry and material properties, may induce large stochastic variations in the system performance metrics of interest. These effects must be carefully assessed and accounted for in robust designs. In this scenario, traditional Monte Carlo-based simulations become a major bottleneck owing to the massive amount of data they typically require.

Therefore, alternative and more efficient strategies were investigated in the past decade. In this regard, a standard and well-recognized approach for stochastic modeling is provided by the polynomial chaos expansion (PCE) framework. These methods approximate the stochastic quantities of interest using polynomial bases that are orthogonal w.r.t. to the distribution of the uncertain parameters [1], thus enabling a precise uncertainty quantification in terms of statistical moments and distribution functions. The PCE framework became widely popular also in the field of electrical engineering [2], e.g., to investigate the impact of process variations in large-scale integration circuits [3]–[17]. The available techniques can be subdivided into two classes: intrusive ones [3]–[8], chiefly

based on the so-called stochastic Galerkin method, favor model accuracy and interpretability at the expense of implementational easiness, as they require access to the system equations and hardly apply to nonlinear problems. On the other hand, collocation approaches [9]–[17] are essentially black box, and merely leverage a collection of responses computed for some suitable configurations of the uncertain parameters, thus similarly to Monte Carlo, but being more parsimonious in the number of samples required.

Regardless of the aforementioned differences, conventional applications make use of single expansions, which are linear in their coefficients. Recently, rational PCEs [18]–[20] were proposed for accuracy improvement in the uncertainty quantification of stochastic linear systems in the frequency domain (FD) [21]. Indeed, the technique was proven to provide a far more accurate model for generic FD network responses, and an exact model for the responses of lumped circuits [22]. The method is non-intrusive and features an iterative re-weighted linear least-square regression for the determination of the expansion coefficients. Compared to the standard single PCE, the main drawback of rational PCEs is the reduced computational efficiency, since in this case the regression matrix to be inverted differs for each frequency point and for each output of interest. This makes the method unsuitable for the characterization of large multi-port structures and/or fine frequency sweeps.

The associate editor coordinating the review of this manuscript and approving it for publication was Wiren Becker[ID].

In order to alleviate this shortcoming, we introduce here a compression strategy, based on principal component analysis (PCA) [23], that allows for a considerable reduction of the number of regression problems to be solved, thus remarkably improving the efficiency in large-size problems. This approach was recently used in conjunction with generic surrogate modeling techniques to improve the efficiency of stochastic time-domain circuit simulations [24]. In this paper, it is adapted for the use with rational PCEs in the FD. Therefore, compared to [24], the main novel contribution is in the use of rational PCEs as surrogate models, which were shown to provide remarkably better accuracy for the uncertainty quantification of FD network responses. Moreover, novel theoretical insights are provided, and the behavior of the PCA coefficients w.r.t. the original stochastic variables is highlighted and discussed. In particular, it is found that optimal accuracy is obtained by matching the expansion order to the number of principal components, when feasible. Several application examples, ranging from a trivial analytical case to distributed circuits and electromagnetic structures, illustrate and validate the advocated approach.

The rest of the paper is organized as follows. Section II summarizes the state of the art of PCE-based surrogate modeling, outlining both standard and rational model structures. Section III introduces the proposed PCA compression. A simple illustrative example is discussed in Section IV, whereas more realistic application test cases are provided in Section V. Finally, conclusions are drawn in Section VI. Throughout the paper, plain x, lowercase bold $\boldsymbol{x}$, and uppercase bold $\mathbf{X}$ variables denote scalar, vector, and matrix quantities, respectively. Superscript $^\mathsf{T}$ stands for transpose and $^\mathsf{H}$ denotes conjugate transpose (Hermitian).

II. STATE-OF-THE-ART POLYNOMIAL CHAOS MODELING

We consider a generic P-port electrical system affected by d uncertain parameters collected in vector $\boldsymbol{\xi} = (\xi_1, \ldots, \xi_d)$. We assume that the FD system response can be evaluated (e.g., through a circuit or field solver), at any frequency and fixed configuration of the uncertain parameters $\boldsymbol{\xi}$.

A. CONVENTIONAL MODEL: SINGLE PCE

In the standard PCE framework [2], any FD port characterization $\mathbf{S}$ at a given complex frequency $s_m \in \{\jmath 2\pi f_m\}_{m=1}^M$ is modeled as the following PCE

$$\mathbf{S}(s_m, \boldsymbol{\xi}) \approx \hat{\mathbf{S}}_m(\boldsymbol{\xi}) = \sum_{\ell=1}^L \mathbf{S}_{m,\ell} \varphi_\ell(\boldsymbol{\xi}), \tag{1}$$

where $\mathbf{S}, \hat{\mathbf{S}}_m, \mathbf{S}_{m,\ell} \in \mathbb{C}^{P \times P}$. The basis functions $\{\varphi_\ell\}_{\ell=1}^L$ are suitable multivariate polynomials that are orthogonal w.r.t. the joint probability density function of $\boldsymbol{\xi}$, as discussed later in Section III. It should be noted that the model (1) is discrete over the frequencies s_m and continuous over the uncertain variables $\boldsymbol{\xi}$. A continuous model also w.r.t. frequency can be obtained by applying vector fitting to the PCE coefficients [25].

The model coefficients are computed by solving the linear regression problem

$$\boldsymbol{x}_{m,ij} = \arg \min_{\boldsymbol{x}} \left\| \boldsymbol{\Psi} \boldsymbol{x} - \boldsymbol{b}_{m,ij} \right\|_2 \tag{2}$$

in the least-square sense over a set $\{\boldsymbol{\xi}_k\}_{k=1}^K$ of samples of the uncertain parameters (typically, randomly drawn), where:

- $\boldsymbol{x}_{m,ij} = (S_{m,ij,1}, \ldots, S_{m,ij,L})^\mathsf{T} \in \mathbb{C}^L$, i.e., a vector collecting all PCE coefficients for the element (ij) of matrix $\mathbf{S}$ at the frequency s_m;
- $\boldsymbol{b}_{m,ij} = \left(S_{ij}(s_m, \boldsymbol{\xi}_1), \ldots, S_{ij}(s_m, \boldsymbol{\xi}_K)\right)^\mathsf{T} \in \mathbb{C}^K$ is a vector collecting the element (ij) of matrix $\mathbf{S}$ evaluated at the frequency s_m for all the regression samples of $\boldsymbol{\xi}$;
- $\boldsymbol{\Psi} \in \mathbb{C}^{K \times L}$ with entries $\Psi_{k,\ell} = \varphi_\ell(\boldsymbol{\xi}_k)$, for $k = 1, \ldots, K$, $\ell = 1, \ldots, L$, i.e., a matrix containing all the basis functions evaluated at the regression samples.

The solution to (2) is well-known and reads

$$\boldsymbol{x}_{m,ij} = \boldsymbol{\Psi}^+ \boldsymbol{b}_{m,ij}, \tag{3}$$

where $\boldsymbol{\Psi}^+ = (\boldsymbol{\Psi}^\mathsf{H} \boldsymbol{\Psi})^{-1} \boldsymbol{\Psi}^\mathsf{H}$ denotes the Moore-Penrose pseudo-inverse [26] of $\boldsymbol{\Psi}$.

At this point, it is important to note that matrix $\boldsymbol{\Psi}$ is independent on the frequency and response matrix element. Therefore, the full characterization of the model (1) can be carried out simultaneously by stacking the regression data $\boldsymbol{b}_{m,ij}$ for all frequency points and port variables into a single matrix

$$\mathcal{B} = \begin{pmatrix} \longleftarrow \boldsymbol{b}_{1,11}^\mathsf{T} \longrightarrow \\ \vdots \\ \longleftarrow \boldsymbol{b}_{M,PP}^\mathsf{T} \longrightarrow \end{pmatrix} \in \mathbb{C}^{MQ \times K}, \tag{4}$$

with $Q = P^2$, and computing

$$\mathcal{X} = \left(\boldsymbol{\Psi}^+ \mathcal{B}^\mathsf{T} \right)^\mathsf{T}, \tag{5}$$

which collects all model coefficients in (1) with the same ordering as in (4).

Despite a remarkable computational efficiency, it was shown in [21] that the model (1) is not very accurate for electrical/electromagnetic systems, especially at high frequency and for distributed and/or strongly resonant structures. Moreover, the number K of regression samples required to "train" the model becomes rapidly prohibitive when the expansion order is increased.

B. RATIONAL PCE MODEL

For the aforementioned reasons, an element-wise rational model of the form

$$S_{ij}(s_m, \boldsymbol{\xi}) \approx \hat{S}_{m,ij}(\boldsymbol{\xi}) = \frac{\sum_{\ell=1}^L N_{m,ij,\ell}\, \varphi_\ell(\boldsymbol{\xi})}{1 + \sum_{\ell=2}^L D_{m,ij,\ell}\, \varphi_\ell(\boldsymbol{\xi})} \tag{6}$$

for $i, j = 1, \ldots, P$, was put forward [21]. In [22], it was further shown that such a model is exact for lumped systems, provided that a suitable truncation strategy is used.

The model coefficients in (6) are obtained through the iterative solution of the linearized regression problem

$$\begin{pmatrix} \boldsymbol{n}_{m,ij}^{\nu} \\ \boldsymbol{d}_{m,ij}^{\nu} \end{pmatrix} = \underset{\boldsymbol{n},\boldsymbol{d}}{\arg\min}$$

$$\left\| \left(\boldsymbol{\Delta}_{m,ij}^{\nu}\boldsymbol{\Psi} - \boldsymbol{\Delta}_{m,ij}^{\nu}\boldsymbol{\Psi}_{m,ij}' \right) \begin{pmatrix} \boldsymbol{n} \\ \boldsymbol{d} \end{pmatrix} - \boldsymbol{\Delta}_{m,ij}^{\nu}\boldsymbol{b}_{m,ij} \right\|_2 \quad (7)$$

in the least-square sense, in which ν denotes the iteration index, $\boldsymbol{\Psi}$ and $\boldsymbol{b}_{m,ij}$ are defined as in (2), and in addition:

- $\boldsymbol{n}_{m,ij}^{\nu} = (N_{m,ij,1}^{\nu}, \ldots, N_{m,ij,L}^{\nu})^{\mathsf{T}} \in \mathbb{C}^L$, i.e., a vector collecting the numerator coefficients at iteration ν;
- $\boldsymbol{d}_{m,ij}^{\nu} = (D_{m,ij,2}^{\nu}, \ldots, D_{m,ij,L}^{\nu})^{\mathsf{T}} \in \mathbb{C}^{L-1}$, i.e., a vector collecting the denominator coefficients at iteration ν;
- $\boldsymbol{\Psi}_{m,ij}' \in \mathbb{C}^{K \times (L-1)}$ with entries $\Psi_{k,\ell}' = S_{ij}(s_m, \boldsymbol{\xi}_k)\Psi_{k,\ell}$, for $k = 1, \ldots, K$, $\ell = 2, \ldots, L$;
- $\boldsymbol{\Delta}_{m,ij}^{\nu}$ is a diagonal matrix collecting the inverse of the denominator PCE at the iteration $\nu - 1$ evaluated at the regression samples. It is initialized to the identity matrix, and updated throughout the iterations as

$$\boldsymbol{\Delta}_{m,ij}^{\nu} = \left[\mathrm{diag}\left\{ \boldsymbol{\Psi} \begin{pmatrix} 1 \\ \boldsymbol{d}_{m,ij}^{\nu-1} \end{pmatrix} \right\} \right]^{-1}.$$

The regression problem (7) has $2L - 1$ unknowns, corresponding to the numerator and denominator PCE coefficients. In [21], a Latin hypercube sampling strategy was used to generate the K random samples of $\boldsymbol{\xi}$ for the regression, and $K \gg 2L - 1$ was taken for the system to be sufficiently overdetermined. The iterative re-weighting is used to eliminate the bias introduced by the linearization [27]. Iterations stop after convergence is detected.

The above-described approach has one important limitation. The regression matrix in (7) depends on both frequency and port response, hence the iterative regression solution must be carried out separately for each frequency point s_m and for each input-output pair (ij). This leads to a possibly large number MQ of separate, independent (and iterative) calculations. Therefore, the approach becomes intractable for the responses of systems with many ports evaluated over a fine frequency sweep. A compression strategy is proposed in the next section to alleviate this problem.

Before continuing, we would like to remark at this point that for reciprocal systems, $S_{ij}(s_m) = S_{ji}(s_m) \; \forall i, j, m$, and therefore the modeling reduces to the triangular part of $\mathbf{S}$, leading to $Q = P(P+1)/2$ unknowns instead of $Q = P^2$. A further reduction may occur for symmetrical structures. In the following, Q will denote in general the actual number of distinct port responses to be modeled. It is important to remark that, however, any redundancy in the data is automatically removed by the compression strategy introduced in the next section.

Throughout the following, we will refer to the ensemble of stochastic responses $\{\mathbf{S}(s_m, \boldsymbol{\xi}_k)\}_{m,k=1}^{M,K}$ that is used to train the model, collected into matrix (4), as the "training dataset".

III. PCA-COMPRESSED POLYNOMIAL CHAOS MODELING

In order to reduce the exorbitant number of MQ regression solutions that is required by the full characterization of the model (6) for all port responses and frequency points, a compression strategy is introduced using PCA [23]. This approach is motivated by the fact that the responses of a linear system exhibit some amount of interdependency between different ports and frequency points, which can be effectively handled by compressing the data into a reduced subset by means of PCA [24].

A. EIGENVALUE-BASED CALCULATION

The approach starts by interpreting the $MQ \times K$ matrix $\mathcal{B}$, defined in (4), as a collection of K realizations of a MQ-variate stochastic variable $\boldsymbol{\beta}$. Next, the experimental covariance matrix of $\boldsymbol{\beta}$, i.e.,

$$\begin{aligned} \mathbf{K}_{\boldsymbol{\beta}} &= \mathbb{E}\{(\boldsymbol{\beta} - \mathbb{E}\{\boldsymbol{\beta}\})(\boldsymbol{\beta} - \mathbb{E}\{\boldsymbol{\beta}\})^{\mathsf{H}}\} \\ &\approx \frac{\sum_{k=1}^{K}(\boldsymbol{\beta}_k - \boldsymbol{\mu}_{\boldsymbol{\beta}})(\boldsymbol{\beta}_k - \boldsymbol{\mu}_{\boldsymbol{\beta}})^{\mathsf{H}}}{K-1} = \frac{\widetilde{\mathcal{B}}\widetilde{\mathcal{B}}^{\mathsf{H}}}{K-1} \end{aligned} \quad (8)$$

is computed, where $\mathbf{K}_{\boldsymbol{\beta}} \in \mathbb{C}^{MQ \times MQ}$, $\boldsymbol{\beta}_k \in \mathbb{C}^{MQ}$ is the kth column of $\mathcal{B}$,

$$\boldsymbol{\mu}_{\boldsymbol{\beta}} = \frac{1}{K}\sum_{k=1}^{K}\boldsymbol{\beta}_k \quad (9)$$

is the mean estimated over the stochastic samples, and

$$\widetilde{\mathcal{B}} = \mathcal{B} - (\boldsymbol{\mu}_{\boldsymbol{\beta}} \otimes \mathbf{1}_{1 \times L}), \quad (10)$$

where $\mathbf{1}_{1 \times L} \in \mathbb{R}^L$ is a row vector of ones.

Given the eigenvalue decomposition of $\mathbf{K}_{\boldsymbol{\beta}}$, i.e.,

$$\mathrm{eig}(\mathbf{K}_{\boldsymbol{\beta}}) = \boldsymbol{\Phi}\boldsymbol{\Lambda}\boldsymbol{\Phi}^{\mathsf{H}}, \quad (11)$$

where $\boldsymbol{\Lambda}$ is a diagonal matrix collecting the eigenvalues $\{\lambda_n\}_{n=1}^{MQ}$ of $\mathbf{K}_{\boldsymbol{\beta}}$, assumed to be sorted in descending order, and $\boldsymbol{\Phi}$ is the corresponding matrix of eigenvectors, the realizations $\{\boldsymbol{\beta}_k\}_{k=1}^{K}$ of the original training dataset can be expressed as [23]

$$\boldsymbol{\beta}_k = \boldsymbol{\mu}_{\boldsymbol{\beta}} + \sum_{n=1}^{MQ} Z_{k,n}\boldsymbol{\phi}_n \quad (12)$$

where $\boldsymbol{\phi}_n$ denotes the nth eigenvector (i.e., the nth column of $\boldsymbol{\Phi}$), whereas the coefficients $Z_{k,n}$ are obtained as

$$Z_{k,n} = \boldsymbol{\phi}_n^{\mathsf{H}}(\boldsymbol{\beta}_k - \boldsymbol{\mu}_{\boldsymbol{\beta}}). \quad (13)$$

The expansion (12) can be truncated to retain only the first $\bar{n}$ eigenvectors, corresponding to the most significant eigenvalues, based on a pre-defined relative threshold. This is the so-called PCA, leading to the approximation

$$\boldsymbol{\beta}_k \approx \hat{\boldsymbol{\beta}}_k = \boldsymbol{\mu}_{\boldsymbol{\beta}} + \sum_{n=1}^{\bar{n}} Z_{k,n}\boldsymbol{\phi}_n \quad (14)$$

of the data in (4). As it will be shown by the application examples, $\bar{n} \ll MQ$ (typically, two to three orders of magnitude less).

Now, the key point is that the collection of the PCA coefficients $Z_{k,n}$ can be seen as a set of K realizations of $\bar{n}$ stochastic variables stemming from (and hence, depending on) the original random parameters $\boldsymbol{\xi}$. As such, each of the $\bar{n}$ PCA coefficients can be represented using the rational PCE model (6) as

$$Z_n(\boldsymbol{\xi}) \approx \frac{\sum_{\ell=1}^{L} N_{n,\ell}\varphi_\ell(\boldsymbol{\xi})}{1 + \sum_{\ell=2}^{L} D_{n,\ell}\varphi_\ell(\boldsymbol{\xi})}, \tag{15}$$

with $n = 1, \ldots, \bar{n}$, and coefficients computed as in (7) using the samples $\{Z_{k,n}\}_{k=1}^{K}$. The fundamental difference, compared to (6), is that (15) requires to construct only $\bar{n}$ rational models, instead of MQ.

Once the model (15) is computed, it is used to generate new random samples for the PCA coefficients in (14), which in turn allows obtaining new samples for the random variables $\boldsymbol{\beta}$. The corresponding samples for the original port variables are recovered by assembling a new dataset $\mathcal{B}$ and reshaping it back to the original form according to (4). It should be noted that the proposed method no longer computes the PCE coefficients of the port variables as in (1) or (6). Samples thereof are instead obtained directly from the rational PCE model (15) of the PCA components. The PCA compression is also applicable in conjunction with the conventional PCE, yet without significant benefit on neither the computational efficiency nor the accuracy, as we will show later on.

B. SVD-BASED CALCULATION

The evaluation of the eigenvalue decomposition (11) is not efficient for very large-sized matrices, which is often the case in practice. Conveniently, the eigenvalue decomposition of the covariance matrix (8) can be reformulated as a singular value decomposition (SVD) [23]. Consider the "economy-size" SVD of the entire zero-meaned training dataset $\widetilde{\mathcal{B}}$

$$\mathrm{svd}(\widetilde{\mathcal{B}}) = \mathbf{U}\boldsymbol{\Sigma}\mathbf{V}^{\mathsf{H}} \tag{16}$$

where, since $MQ > K$, $\mathbf{U} \in \mathbb{C}^{MQ \times K}$, $\boldsymbol{\Sigma} \in \mathbb{R}^{K \times K}$ is a diagonal matrix collecting the singular values $\{\sigma_n\}_{n=1}^{K}$ of $\widetilde{\mathcal{B}}$ in descending order, and $\mathbf{V} \in \mathbb{C}^{K \times K}$. Recalling that the singular values of a matrix $\mathbf{M}$ correspond to the square root of the eigenvalues of $\mathbf{M}\mathbf{M}^{\mathsf{H}}$, and that the left-singular vectors are a set of corresponding orthonormal eigenvectors [26], then the eigenvalues in (11) are related to the singular values in (16) by

$$\lambda_n = \frac{\sigma_n^2}{K - 1} \tag{17}$$

whereas the eigenvectors (columns of $\boldsymbol{\Phi}$) and the left-singular vectors (columns of $\mathbf{U}$) are proportional up to a complex constant with unit magnitude, and hence they are interchangeable in (12)–(14). Because of (17), a relative threshold ϵ on the singular values of $\widetilde{\mathcal{B}}$ is equivalent to a relative threshold ϵ^2 on the eigenvalues of $\mathbf{K}_{\boldsymbol{\beta}}$.

C. ERROR OF PCA TRUNCATION

First of all, we assume all the training samples in dataset $\mathcal{B}$ to be an exact representation of the true system response, with no associated "measurement error". Let us consider a PCA truncation based on a relative threshold ϵ on the singular values of the zero-meaned dataset $\widetilde{\mathcal{B}}$. We denote with $\widehat{\mathcal{B}}$ the corresponding approximation of $\mathcal{B}$, i.e., a matrix collecting columnwise the approximated samples $\{\hat{\boldsymbol{\beta}}_k\}_{k=1}^{K}$ in (14), and with $\mathbf{K}_{\hat{\boldsymbol{\beta}}}$ the corresponding experimental covariance matrix. Thanks to the properties of singular values [28], the following relations hold for the approximation error:

$$\|\widehat{\mathcal{B}} - \mathcal{B}\|_2 \equiv \sigma_{\bar{n}+1} = \frac{\sigma_{\bar{n}+1}}{\sigma_1}\|\widetilde{\mathcal{B}}\|_2 \le \epsilon\|\widetilde{\mathcal{B}}\|_2 \tag{18}$$

where $\sigma_{\bar{n}+1}$ is the first discarded singular value, and the standard matrix 2-norm $\|\mathbf{M}\|_2 = \max(\sigma(\mathbf{M})) = \sigma_1$ has been used. Moreover, using (17), the error on the covariance matrix can be expressed as

$$\|\mathbf{K}_{\hat{\boldsymbol{\beta}}} - \mathbf{K}_{\boldsymbol{\beta}}\|_2 \equiv \frac{\sigma_{\bar{n}+1}^2}{K-1} = \left(\frac{\sigma_{\bar{n}+1}}{\sigma_1}\right)^2 \|\mathbf{K}_{\boldsymbol{\beta}}\|_2 \le \epsilon^2\|\mathbf{K}_{\boldsymbol{\beta}}\|_2. \tag{19}$$

Finally, the following property holds for the root-mean-square error (RMSE) over the individual realizations $\boldsymbol{\beta}_k$:

$$\sqrt{\frac{1}{K}\sum_{k=1}^{K}\|\hat{\boldsymbol{\beta}}_k - \boldsymbol{\beta}_k\|_2^2} = \frac{1}{\sqrt{K}}\|\widehat{\mathcal{B}} - \mathcal{B}\|_F \le \|\widehat{\mathcal{B}} - \mathcal{B}\|_2$$
$$\le \epsilon\|\widetilde{\mathcal{B}}\|_2, \tag{20}$$

where $\|\cdot\|_F$ denotes the Frobenius norm and the property $\|\mathbf{M}\|_F \le \sqrt{r}\|\mathbf{M}\|_2$, where $r \le K$ is the rank, has been used. Therefore, the PCA approximation error is rigorously controlled by means of the truncation threshold. It should be noted that the overall approximation error is the sum of the contributions of the PCA truncation and of the PCE approximation of the PCA coefficients, which is in turn controlled by letting the expansion order be sufficiently high.

D. PCE TRUNCATION

Without loss of generality, we assume the components of the random vector $\boldsymbol{\xi}$ be independent and identically distributed (i.i.d.), with probability density function (PDF) $w(\xi)$. In this case, the basis functions in the PCE are constructed as the product

$$\varphi_\ell(\boldsymbol{\xi}) = \prod_{j=1}^{d} \zeta_{\alpha_j}(\xi_j), \tag{21}$$

where $\{\zeta_\alpha(\xi)\}_{\alpha=0}^{\infty}$ are univariate polynomials of degree α satisfying the orthogonality condition

$$\int_{\mathbb{R}} \zeta_\alpha(\xi)\zeta_\gamma(\xi)w(\xi)d\xi = 0, \quad \alpha \ne \gamma. \tag{22}$$

An implicit mapping is introduced between the scalar index ℓ and a vector of univariate degrees $\boldsymbol{\alpha} = (\alpha_1, \ldots, \alpha_d)$ in (21).

With the above definitions, three truncation strategies of increasing sparsity are typically defined for the PCE [2], [29], given an expansion order p:

- tensor product (TP), such that $\|\boldsymbol{\alpha}\|_\infty \leq p$ and leading to $L = (p + 1)^d$ terms;
- total degree (TD), such that $\|\boldsymbol{\alpha}\|_1 \leq p$ and leading to $L = (p + d)!/(p!d!)$ terms;
- hyperbolic, such that $\|\boldsymbol{\alpha}\|_u \leq p$, with $0 < u < 1$.

The above truncation strategies are equivalent for the univariate case ($d = 1$).

A TD truncation is typically used for conventional single PCE models [2], since the higher-order interactions included in a TP of the same degree are often negligible. On the other hand, it was shown that using a TP truncation of order $p = 1$ for both the numerator and denominator of a rational model yields an exact model for lumped circuits [22]. Because of the PCA transformation, however, the exactness no longer holds for the PCA coefficients in (15), even for lumped systems. Therefore, whereas in [21] the above property motivated, by extension, the choice of a TP truncation also for distributed systems, although generally with $p > 1$, here we will also consider the more compact TD truncation for the rational model (15).

E. SAMPLING STRATEGY

Low-discrepancy sequences are frequently used in quasi-Monte Carlo simulations to speed-up the convergence of sampling-based techniques [30]. They are fully deterministic sequences of multivariate samples with optimal space-filling properties. Two notable examples thereof are the Sobol [31] and Halton [32] sequences. Their samples, which we denote with $\{(\eta_{1,k}, \ldots, \eta_{d,k})\}_{k=1}^K$, are uniformly distributed in the hypercube $[0, 1]^d$. Normally-distributed samples are obtained through the inverse probability transform [33]

$$\xi_{j,k} = F_{\mathcal{N}}^{-1}(\eta_{j,k}), \quad \forall j, k \tag{23}$$

where $F_{\mathcal{N}}^{-1}$ is the inverse of the cumulative density function of the standard normal distribution. It is important to mention that the first element of the sequence is always the origin and it has to be discarded when transforming into a normal distribution, since $F_{\mathcal{N}}^{-1}(0) = -\infty$. This operation involves a negligible computational cost. Hence, we did not consider alternative methods, such as the Box-Muller transform [34], for improving the computational efficiency.

Figure 1 shows the distribution of $K = 100$ bivariate ($d = 2$) Gaussian samples drawn according to plain random number generation (like in standard Monte Carlo), Latin hypercube sampling, Sobol sequence, and Halton sequence. The samples from the low-discrepancy sequences are more evenly spread in the space. In this paper, we draw training samples according to a Sobol sequence in place of the Latin hypercube sampling strategy used in [21].
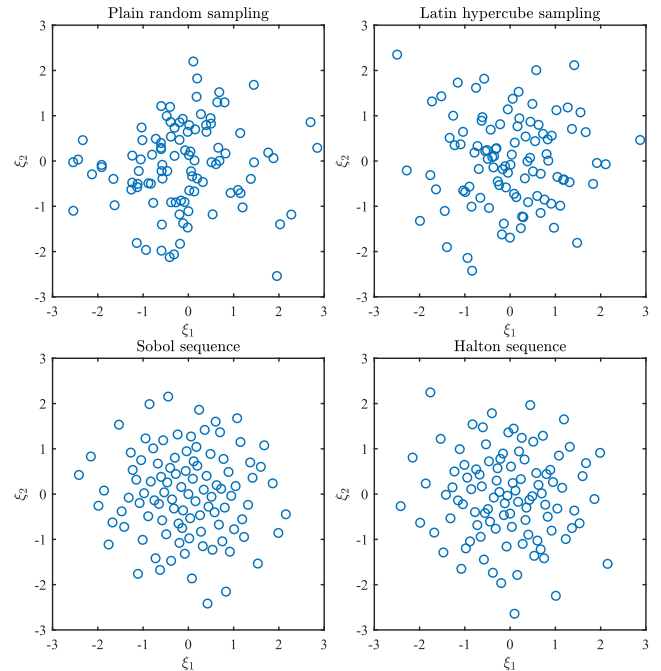

FIGURE 1. Distribution of $K = 100$ bivariate Gaussian samples drawn according to different schemes.

IV. ILLUSTRATIVE EXAMPLE

We start by considering a trivial analytical example consisting of a parallel RLC circuit, whose impedance reads

$$Z(s) = \frac{sRL}{R + sL + s^2 RLC}. \tag{24}$$

Given the rational form of (24), and contrary to the conventional single PCE, a first-order rational PCE (6) with TP truncation is exact, as was rigorously proven for the general case in [22].

We start by considering a univariate case in which only the inductance L is uncertain, following a Gaussian distribution with a nominal value of 3 H and a standard deviation of 0.6 H (i.e., 20% relative). The resistance is $R = 2\,\Omega$ and the capacitance is $C = 4$ F. For the calculation of the model coefficients, we consider $K = 50$ impedance samples evaluated for inductance values generated from a Sobol sequence.

We first illustrate the impact of the PCA compression on the classical, single PCE. Therefore, we assess the modeling error for different PCA truncation thresholds and PCE orders. Figure 2 shows the behavior of the root-mean-square error (RMSE), calculated over 10000 samples of the stochastic inductance. The average and maximum error over frequency, obtained by applying the PCE directly to FD data (dashed yellow lines), are compared against the results achieved in conjunction with PCA compression of the training dataset with various truncation thresholds on the singular values, namely $\epsilon = \{10^{-2}, 10^{-3}, 10^{-4}, 10^{-5}\}$ (solid red lines). It is noted that the error does not monotonically decrease with increasing order. This is because the model coefficients of higher-order expansions are computed with lower
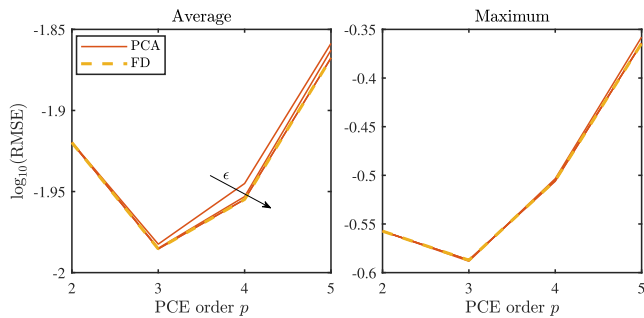
FIGURE 2. Average (left) and maximum (right) RMSE over frequency obtained with single PCEs of various orders, applied to FD data (dashed yellow lines) or in conjunction with PCA compression with different truncation thresholds (solid red lines).
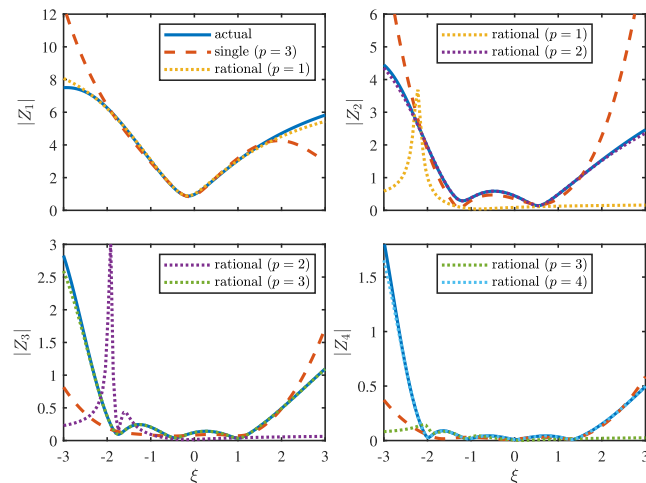

FIGURE 3. Magnitude of the PCA coefficients for the impedance of the parallel RLC circuit with uncertain inductance. Blue solid lines: actual value; red dashed line: single PCE model of order $p = 3$; yellow, purple, green, and cyan dotted lines: rational PCE models of order $p = 1, 2, 3, 4$, respectively.

accuracy (or higher variance) with a given training dataset, since the number of unknowns to be estimated by the regression increases. This phenomenon is called the "bias-variance tradeoff" in statistical learning theory [35], and can be mitigated using LASSO or Ridge regressions. It was observed in [21] that the number of required samples increases superlinearly with the number of unknown coefficients to estimate, thus making the use of high-order classical PCEs impractical for the modeling of FD responses. Moreover, the PCA truncation threshold is found to have little influence, especially on the maximum error. From $\epsilon = 10^{-4}$ and below, the FD and PCA-compressed solutions provide the same accuracy up to the fourth digit, meaning that the PCA compression error has become practically negligible compared to the PCE error. The error of a first-order rational PCE model is found instead to be limited to machine precision, as expected.

Next, we focus on the proposed modeling scheme, i.e., the PCA-compressed rational approximation discussed in Section III. We first investigate the accuracy of the representation (15) of the principal components, for different expansion orders of the numerator and denominator, and then we analyze the resulting accuracy on the impedance. To this end, we start by considering a PCA compression with a truncation threshold of $\epsilon = 10^{-2}$. This leads to retaining $\bar{n} = 4$ PCA coefficients out of the 501 original frequency samples, with a reduction to a mere 0.8% of the original data. Figure 3 reports a parametric analysis of the four PCA coefficients $\{Z_n\}_{n=1}^4$ as a function of the normalized inductance value, denoted with ξ. The solid blue lines show the magnitude of the actual value of Z_n, obtained by projecting the corresponding impedance samples via (13). The dashed red lines are single PCE models of order $p = 3$, which yield the best model accuracy according to Fig. 2, and yet exhibit a rather large error for all PCA coefficients, especially for $|\xi| > 2$.[1] The dotted curves are rational PCE models of various orders. In particular, each panel shows the rational models of order $p = n - 1$ and $p = n$. This comparison leads to the interesting observation that a nth-order rational

PCE model is very accurate for the nth coefficient Z_n, whereas a rather large error is observed if a lower order is used. More precisely, models of order $p \leq n - 1$ result to be highly inaccurate, whereas using $p \geq n$ ensures excellent accuracy. Therefore, the order of the PCA coefficients seems to increase linearly with the index.

This is further confirmed by the plots in Fig. 4, which now report the average and maximum RMSE on the FD impedance obtained by applying a rational PCE in conjunction with PCA compression, for different expansion orders and truncation thresholds. The dots mark the point at which the expansion order p matches the number of principal components $\bar{n}$ for the corresponding truncation threshold. It is indeed noted that the accuracy does not significantly improve by further increasing the expansion order beyond that value. This corroborates the conclusion that such model is virtually exact, with the residual error on the impedance being due to the PCA truncation. Moreover, there is no significant difference in using different truncation thresholds when $p < \bar{n}$.
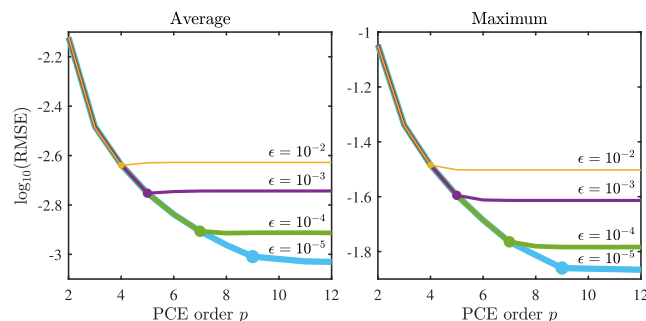

FIGURE 4. Average (left) and maximum (right) RMSE over frequency obtained with rational PCEs of various orders, applied in conjunction with PCA compression with different truncation thresholds. The dots mark the point at which the expansion order matches the number of principal components.

---

[1]Since ξ is Gaussian distributed, the probability that $|\xi| > 2$ is below 5%, whereas the probability that $|\xi| > 3$ is below 0.3%.

Table 1 summarizes the key figures concerning the accuracy for the various cases. The first row reports the best accuracy that is achieved with a single PCE, i.e., by using order $p = 3$. As already noted, no significant difference is found by applying the PCE directly in the FD or to the PCA-compressed variables. A rational model in the FD is exact, thereby leading to a vanishing error. A very good accuracy is still attained by applying the rational model to the PCA compressed variables. As noted from Fig. 4, the error saturates at $p = \bar{n}$. However, compared to a single PCE, a lower error is obtained also for $p < \bar{n}$ (regardless of the truncation threshold), as is shown, e.g., for the case with $p = 3$. Indeed, albeit no longer being exact, a rational PCE applied in conjunction with PCA compression provides a modeling error that is about one order of magnitude lower than the one obtained with the conventional single PCE.

TABLE 1. Accuracy of various PCE models for the impedance of the parallel RLC circuit with uncertain inductance.

Method	PCA threshold	Order p	RMSE avg	RMSE max
Single PCE	—	3	1.0343×10^{-2}	2.5870×10^{-1}
FD rational PCE	—	1	≈ 0	≈ 0
PCA-compressed rational PCE	$\epsilon = 10^{-2}$	3	3.2645×10^{-3}	4.5731×10^{-2}
	$\epsilon = 10^{-2}$	$\bar{n} = 4$	2.2920×10^{-3}	3.2751×10^{-2}
	$\epsilon = 10^{-3}$	$\bar{n} = 5$	1.7682×10^{-3}	2.5408×10^{-2}
	$\epsilon = 10^{-4}$	$\bar{n} = 7$	1.2403×10^{-3}	1.7206×10^{-2}
	$\epsilon = 10^{-5}$	$\bar{n} = 9$	9.7891×10^{-4}	1.3807×10^{-2}

We perform a similar analysis by now considering all three RLC elements to be uncertain, each with a Gaussian distribution and a 20% relative standard deviation. For the regression, we take $K = 1200$ samples, again from a Sobol sequence and deliberately high for the regressions with various expansion orders to be sufficiently overdetermined. We first consider a direct FD modeling with both a single and a rational PCE. The former is computed using a TD truncation of order $p = 5$, which yields the best accuracy with the given training dataset. For the latter, a first-order TP truncation is used, yielding again an exact model. The corresponding RMSEs are provided in the first two rows of Table 2.

We then apply a PCA compression using a threshold of $\epsilon = 10^{-2}$. As a result of the increased variability caused by the two additional uncertain elements, $\bar{n} = 8$ terms are now retained. Figure 5 shows the scatter plots pairing the magnitude of the PCA coefficients $\{Z_n\}_{n=1}^{8}$, calculated from 101 impedance samples using (13), with the corresponding values obtained using various rational PCE models. Specifically, each plot shows the prediction of a rational model with TP truncation of order $p = n - 1$ (with the exception of the plot for Z_1, as $p = 0$ would correspond to a constant function), a TD truncation of order $p = n$, and a TP truncation of order $p = n$. Keeping in mind that an accurate model results in the points to be aligned along the bisector $y = x$ (dashed line), Fig. 5 allows us to draw the following conclusions:
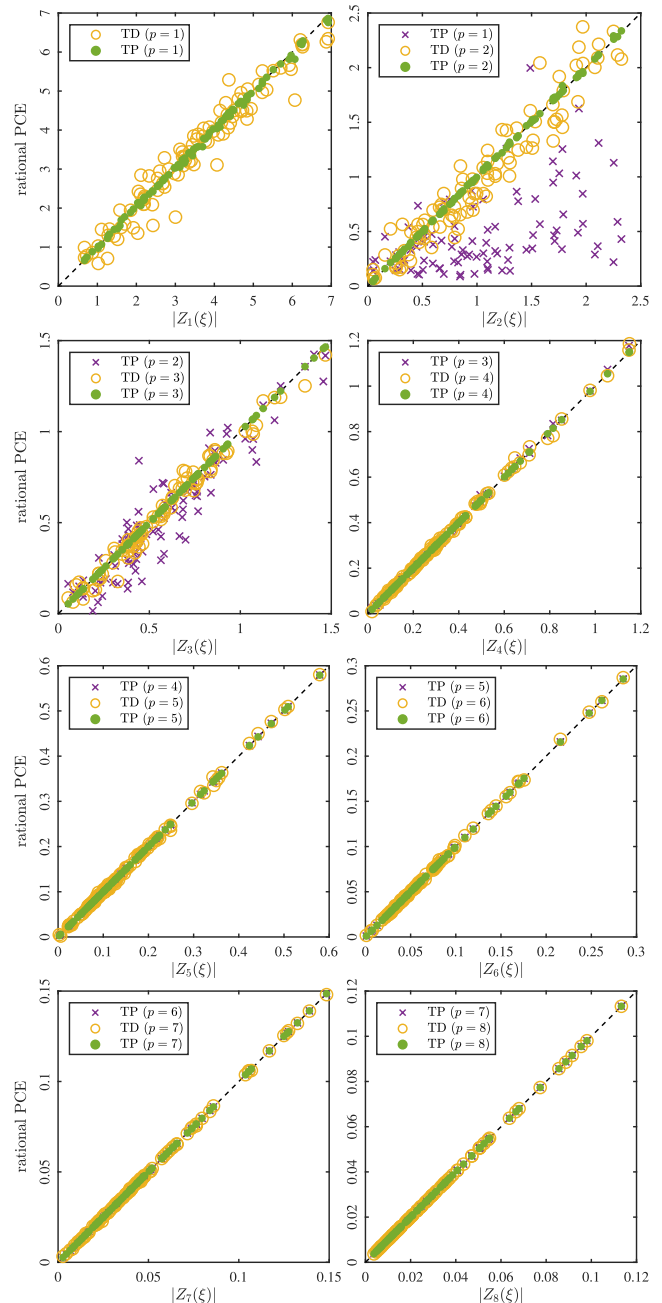

FIGURE 5. Scatter plots of the PCA coefficients Z_n for the impedance of the parallel RLC circuit with three uncertain elements (rational PCE model vs actual value). Cross, circle, and dot markers: $(n - 1)$th-order TP, nth-order TD, and nth-order TP models, respectively.

- A TP rational PCE of order $p = n$ virtually provides an exact model for the corresponding PCA coefficient Z_n, similarly to the univariate case;
- A TD truncation of order $p = n$ also provides an acceptable model for higher-index PCA coefficients.

The appropriateness of the rational models of matching order is further confirmed by the rapid convergence of the iterative regression scheme, which does not occur for $p < n$.

Table 2 provides the information on the RMSE achieved by using rational PCEs in conjunction with PCA compression.

TABLE 2. Accuracy of various PCE models for the impedance of the parallel RLC circuit with all uncertain elements.

Method	PCA threshold	Order p	RMSE avg	RMSE max
Single PCE	—	5	1.1193×10^{-2}	2.3417×10^{-1}
FD rational PCE	—	1	≈ 0	≈ 0
PCA-compressed rational PCE	$\epsilon = 10^{-2}$	5	5.1425×10^{-3}	3.1039×10^{-2}
		$\bar{n} = 8$	2.0102×10^{-3}	1.3109×10^{-2}
	$\epsilon = 10^{-3}$	$\bar{n} = 12$	1.1815×10^{-3}	8.2125×10^{-3}

FIGURE 6. Schematic of the nine-port network with coupled microstrip lines [21], with port definition.

The best compromise on the accuracy is found by using a TD truncation and letting $p = \bar{n}$ for all PCA coefficients, although a marginal saving in computational cost could be attained by tuning the order for each individual Z_n. Compared to single PCEs, a lower error is again achieved with rational PCEs, even when $p < \bar{n}$ is used.

V. APPLICATION EXAMPLES

In this section, we confirm the previous results through the application of the proposed method to more meaningful examples. All the structures are deliberately taken from the existing literature.

We assess the performance based on the achieved RMSE and on the ability of accurately reproducing probability distributions at a specific frequency. In addition, we show that very good accuracy is usually obtained also for the entire FD response for some specific random parameter configurations, even though PCE-based methods tend to favor global statistical accuracy on a large ensemble of parameter configurations, at the expense of the accuracy on specific realizations.

All simulations are performed on a Dell Precision 5820 workstation with an Intel(R) Core(TM) i9-7900X, CPU running at 3.30 GHz, and 32 GB of RAM.

A. NETWORK OF COUPLED TRANSMISSION LINES

We consider here the nine-port network with coupled microstrip lines analyzed in [21]. The structure is shown in Fig. 6 and consists of three sections with coupled microstrip lines interconnected by lumped elements. Because of reciprocity, the number of distinct port variables that needs to be considered is $Q = 45$. We simulate the S-parameters of the network with HSPICE at $M = 401$ equally-spaced frequency points from dc to 20 GHz. Hence, the naive calculation of rational PCE models for all S-parameters requires $MQ = 18045$ separate solutions of the linearized regression (7). For the error assessment, we calculate 5000 samples of the scattering matrix.

In a first instance, we assume a uniform variability of the length of the microstrip lines, in the interval [2.4, 3.6] cm, and we compute $K = 30$ training samples using a Sobol sequence. Then, we apply a PCA compression to the training dataset using a threshold of $\epsilon = 10^{-2}$ on the singular values. This leads to retaining only $\bar{n} = 8$ principal components, i.e., less than 0.05% of the original data. Figure 7 shows
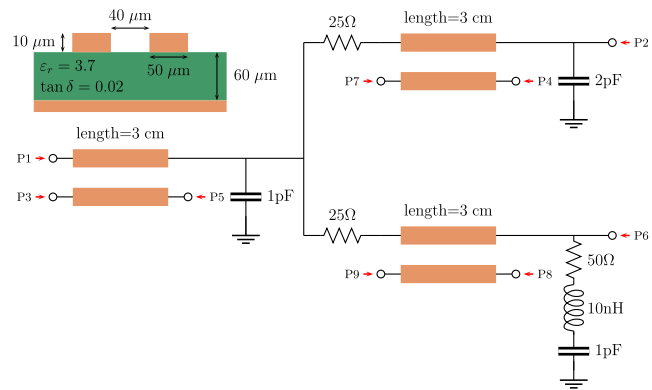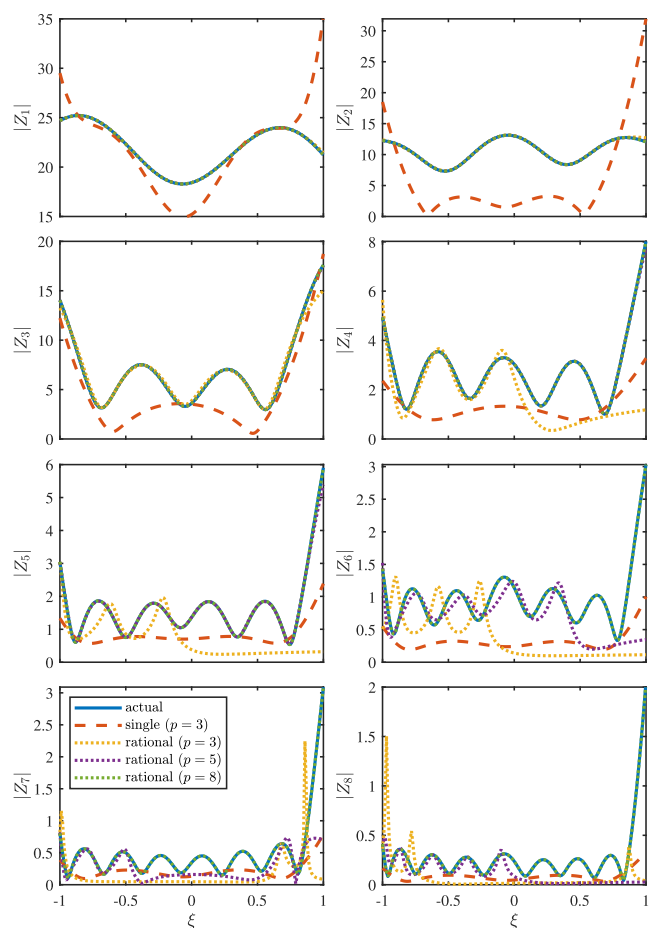

FIGURE 7. Magnitude of the PCA coefficients for the S-parameters of the network with coupled microstrip lines of uncertain length. Blue solid lines: actual value; red dashed lines: single PCE model of order $p = 3$; yellow, purple, and green dotted lines: rational PCE models of order $p = 3$, $p = 5$, and $p = 8$, respectively.

the behavior of the PCA coefficients (solid blue lines) as a function of the normalized length ξ, and compares it against a single PCE model of order $p = 3$ (dashed red line), which yields the lower maximum RMSE with the given training data, and rational PCE models of order $p = 3$, $p = 5$,

TABLE 3. Accuracy and computational times of various PCE models for the S-parameters of the network with coupled microstrip lines of uncertain length.

Method	PCA threshold	Order p	RMSE avg	RMSE max	Training time	Evaluation time	Total CPU time	Speed-up w.r.t. FD
FD single PCE	—	3	4.7618×10^{-2}	4.8058×10^{-1}	< 0.1 s	1.4 s	1.5 s	—
FD rational PCE	—	3	4.9448×10^{-3}	3.0672×10^{-1}	6.6 s	2.6 s	9.2 s	—
		8	2.3993×10^{-5}	3.4468×10^{-3}	13.0 s	2.6 s	15.7 s	—
		11	2.3897×10^{-6}	3.4709×10^{-4}	22.7 s	2.6 s	25.3 s	—
PCA-compressed single PCE	$\epsilon = 10^{-3}$	3	4.7618×10^{-2}	4.8058×10^{-1}	< 0.1 s	0.6 s	0.7 s	$2.2\times$
PCA-compressed rational PCE	$\epsilon = 10^{-2}$	3	1.3531×10^{-2}	1.8324×10^{-1}	< 0.1 s	0.8 s	0.9 s	$10.4\times$
	$\epsilon = 10^{-2}$	8	1.2224×10^{-3}	2.3190×10^{-2}	< 0.1 s	0.8 s	0.9 s	$18.3\times$
	$\epsilon = 10^{-3}$	11	3.4312×10^{-4}	7.1074×10^{-3}	< 0.1 s	0.8 s	0.9 s	$28.2\times$

and $p = \bar{n} = 8$ (dotted yellow, purple, and green lines, respectively). It is confirmed that a rational model of a given order is accurate up to the PCA coefficient of the same index, and that choosing an order that matches the number of retained PCA coefficients ensures high overall accuracy. The conventional single PCE model exhibits a large error for all PCA coefficients instead.

Next, we lower the PCA truncation threshold to $\epsilon = 10^{-3}$, which leads to $\bar{n} = 11$. In the top and bottom-left panels of Fig. 8, we compare some random samples of a subset of S-parameters from the reference HSPICE simulation (solid blue lines) with the predictions obtained using a conventional single PCE of order $p = 3$, applied directly to the FD data (dashed red lines), and the proposed PCA-compressed rational models of order $p = \bar{n} = 11$ (dotted green lines). A remarkably better accuracy is obtained with the latter approach, whereas the former is accurate only at low frequencies. The bottom-right panel shows instead the RMSE over the 5000 reference samples achieved by the conventional single PCE and by the PCA-compressed rational models (solid red and dashed green lines, respectively), for all the 45 distinct S-parameters. As in the previous examples, applying a single PCE in conjunction with PCA compression provides similar accuracy. On the other hand, it is confirmed that the rational models provides a model that is orders of magnitude more accurate.

Table 3 provides the main figures concerning the accuracy and computational time of the various approaches, including the direct FD application of rational PCEs as in [21]. This approach is still feasible for this one-dimensional example, but the processing time is already over $10\times$ higher than with the corresponding PCA-compressed model. The computational cost of the latter is comparable to the more efficient (yet inaccurate) single PCE, for which the computational gain achieved with the PCA-compression is marginal (about $2\times$). The largest gain achieved by the PCA compression is on the model training (i.e., the calculation of the model coefficients through regression), but it does yield an improvement also on the model evaluation time.

It is further established that rational PCE models provide far superior accuracy compared to the conventional single PCE models. As was already observed in Section IV, it is
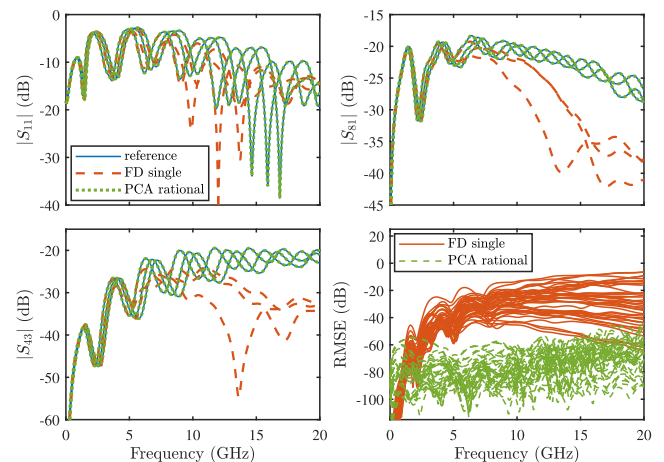

FIGURE 8. Top and bottom-left panels: comparison between a subset of actual S-parameter samples (solid blue lines) of the network with coupled microstrip lines of uncertain length and their PCE models (dashed red lines: conventional FD single PCE model of order $p = 3$; dotted green lines: PCA-compressed rational PCE model of order $p = 11$). Bottom-right panel: RMSE error for all S-parameters (solid red lines: FD single PCE; dashed green lines: rational PCE with PCA compression).

found that taking $p > \bar{n}$, or lowering the PCA truncation threshold without increasing the expansion order accordingly, do not substantially improve the accuracy (results not shown in the table). Finally, it is confirmed that similar accuracy is attained when applying a conventional single PCE model to FD and PCA-compressed data.

Next, we consider the same network but with uncertainty in the substrate thickness and relative permittivity, both following a Gaussian distribution with a 10% relative standard deviation. For training the models, we use $K = 100$ samples from a bivariate Sobol sequence (cfr. Fig. 1). By setting a PCA truncation threshold of $\epsilon = 10^{-3}$, the training dataset is reduced to $\bar{n} = 14$ principal components. We use a TD truncation for both single and rational PCE models. As already noted, for this distributed structure, the use of a more "expensive" (in terms of unknowns) TP truncation for rational models is not motivated by their exactness, not even in the FD as opposed to the lumped case in Section IV.

Figure 9 reports the average (left panel) and maximum (right panel) RMSE, calculated over 5000 samples of the
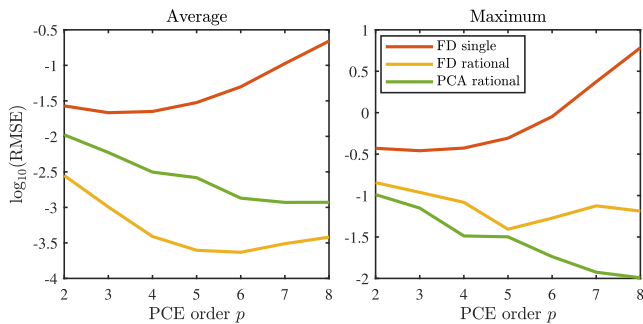
FIGURE 9. RMSE of the FD single PCE (red lines), FD rational PCE (yellow lines), and PCA-compressed rational PCE (green lines) for the network with coupled microstrip lines and uncertain substrate thickness and permittivity, as a function of the PCE order. Left and right panels refer to the average and maximum error over frequency and port, respectively.

S-parameters, obtained with various PCE models of increasing order. In particular, the expansion order is increased until the training of the rational models becomes unfeasible, i.e., the pertinent regression problem is underdetermined). This occurs at a lower expansion order compared to single PCEs, given the higher number of unknowns (almost double). With the available data, it is not possible to match the order of the rational model with the number of retained PCA coefficients, since $L = 120$ for $p = \bar{n} = 14$, and therefore $K < 2L - 1$.

It is observed that the error of the single PCE (red lines) steadily increases for expansion orders above three. Once again, this is a classical manifestation of the bias-variance tradeoff. On the other hand, the error of the rational PCE models is always well below the error of the single PCEs. It is also interesting to note that the PCA-compressed model achieves higher average RMSE compared to the direct FD modeling, but lower maximum RMSE. This is readily explained by the fact the iterative re-weighed regression (7) can locally exhibit poor convergence, and hence a relatively larger error, at some specific frequencies. However, these artifacts are "smoothed out" when working on the compressed data, with PCA intrinsically acting as a regularizer.

Figure 10 compares the PDF of a selection of S-parameters, computed at 18 GHz with the same three methods. Specifically, the distribution of the reference samples (histogram) is compared against the PDFs obtained with a FD single PCE of order $p = 3$ (solid red lines), a FD rational PCE of order $p = 5$ (dashed yellow lines), and a PCA-compressed rational PCE of order $p = 8$ (dashed green lines). These models provide the best accuracy with the given training data, according to Fig. 9. The FD and PCA-compressed rational models provide similar accuracy, which is far better than the one attained with a single PCE. However, the FD model takes 138.2 s for the training, as opposed to a mere 0.6 s required by the advocated PCA-compressed method.

To better investigate the efficiency of the proposed method, Table 4 compares the computational times for training the rational models of increasing order considered in Fig. 9. The processing time of the PCA-compressed models remains
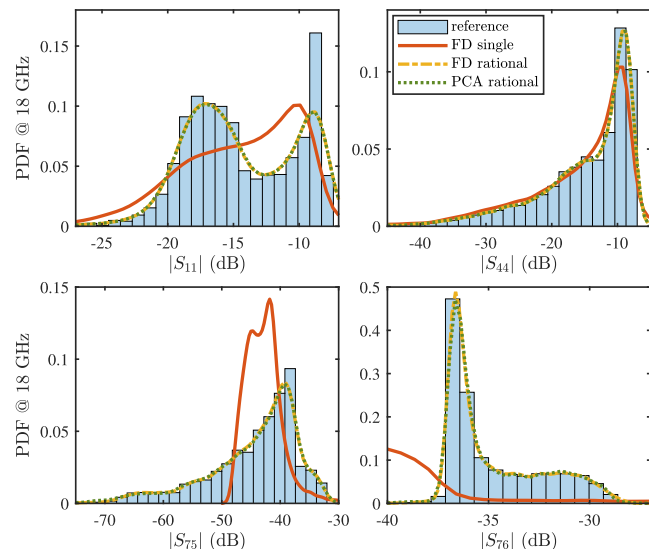

FIGURE 10. PDF of a subset of S-parameters of the network with coupled microstrip lines and uncertainty in the substrate thickness and permittivity, computed at 18 GHz. The distribution of the reference samples (histogram) is compared to the predictions obtained with a single PCE of order $p = 3$ (solid red line), a FD rational PCE of order $p = 5$ (dashed yellow line), and a rational PCE of order $p = 8$ in conjunction with PCA compression (dashed green line).

TABLE 4. Training times of the rational PCE models for the S-parameters of the network with coupled microstrip lines of uncertain substrate thickness and permittivity.

PCE order	2	3	4	5	6	7	8
FD	24.5 s	24.7 s	39.1 s	138.2 s	337.1 s	537.3 s	454.0 s
PCA	0.2 s	0.2 s	0.3 s	0.3 s	0.2 s	0.3 s	0.6 s
Speed-up	137×	130×	149×	472×	1400×	1593×	823×

feasible and within seconds, whereas the construction in the FD rapidly scales up to several minutes. For this very reason, the analysis in [21] was limited to a small subset of S-parameters. For this test case, the PCA compression leads to a speed-up of two to three order of magnitudes.

B. COUPLED-LINE MICROSTRIP BANDPASS FILTER
The next test case considers the coupled-line bandpass filter investigated in [36], consisting of six microstrip resonators and shown in Fig. 11. The structure consists of a perfect electric conductor (PEC) cover, an alumina layer with a thickness of 0.635 mm, relative permittivity $\varepsilon_r = 9.9$, and loss tangent $\tan \delta = 0.0009$, and a gold layer with a thickness of 0.178 mm. Two-port S-parameters, evaluated with the Keysight Advanced Design System (ADS) Momentum simulator at $M = 300$ frequency points from 1 GHz to 7 GHz, are available for 400 configurations of the width of the inner microstrip sections W and their gap S, both in the range [0.635, 0.889] mm and evaluated on a uniform 20×20 grid.

We consider the two parameters to be uniformly distributed, and we use Legendre polynomials as basis functions. We use half of the points (i.e., $K = 200$) as training samples, and the remainder of the points as validation samples. Specifically, we select the training samples as the available
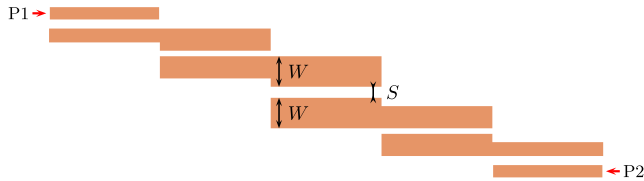
FIGURE 11. Top view of the coupled-line bandpass filter [36].

configurations that lie the closest to the first 200 points of the Sobol sequence. The result is illustrated in Fig. 12, where filled dots and circles denote training and validations samples, respectively, in normalized units. Choosing a PCA truncation threshold of $\epsilon = 10^{-3}$ leads to $\bar{n} = 11$. A rational model of matching order has $L = 78$ terms and can be therefore feasibly trained.
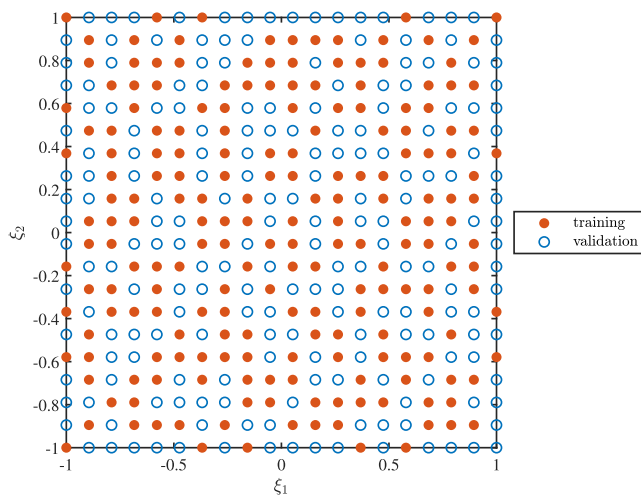

FIGURE 12. Training (red dots) and validation (blue circles) parameter samples for the microstrip bandpass filter.

Figure 13 shows the comparison between the reference S-parameters (solid blue lines) and the corresponding predictions obtained with the PCA-compressed rational model (dashed green lines) for a selection of five validation points. In addition, the dotted red line shows the RMSE over the 200 validation samples, which turns out to be well below -50 dB outside the bandpass region. The mean and maximum RMSE over frequency and ports are 1.3587×10^{-3} and 1.3840×10^{-2}, respectively. The training of the $\bar{n} = 11$ rational models for the principal components requires 2.1 s.

C. PATCH ANTENNA

This example refers to the patch antenna analyzed in [37] and shown in Fig. 14. The patch has a size of 16×12.5 mm. The dielectric layer has a thickness of 0.794 mm and relative permittivity $\varepsilon_r = 2.213$. One-port S-parameters (reflection loss), evaluated again with the ADS Momentum solver at $M = 250$ frequency samples from 1 MHz to 20 GHz, are available for 1000 combinations, on a $10 \times 10 \times 10$ cube,
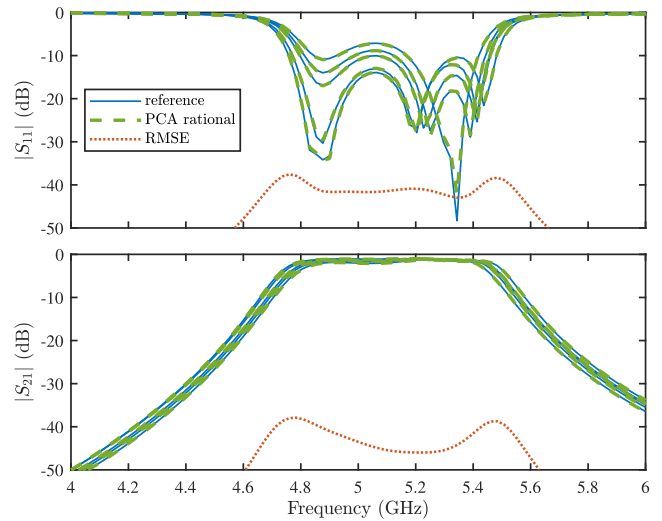

FIGURE 13. S-parameters of the coupled-line microstrip bandpass filter. Solid blue lines: reference responses from ADS Momentum; dashed green lines: predictions of the PCA-compressed rational model; dotted red lines: RMSE error over all the validation samples.

FIGURE 14. Top view of the patch antenna [37].

of the three parameters indicated in Fig. 14, namely the feed stub length $L \in [4, 10]$ mm, width $W \in [2.5, 4]$ mm, and offset $S \in [7, 9]$ mm. Like in the previous example, a subset of samples (250, in this case) that lie the closest to the Sobol sequence, are selected as training data, and the remaining 750 samples are used for validation. We apply a PCA compression with a truncation threshold of $\epsilon = 10^{-2}$, which leads to $\bar{n} = 15$. In this case, it is unfeasible to train a model of matching order, which would have $L = 816$ terms at the numerator and denominator. We therefore consider an expansion order of $p = 5$ and a TD truncation.

Figure 15 provides the comparison for a selection of S-parameter samples. As before, solid blue lines are the reference S-parameters from the ADS simulation, the dashed green lines are the corresponding predictions obtained with the PCA-compressed rational model, and the dotted red line is the RMSE over all the validation samples. Despite using a non-optimal expansion order, very good agreement is again established, with an average and maximum RMSE over frequency of 3.5831×10^{-2} and 6.0897×10^{-2}, respectively. The model training takes 2.5 s.
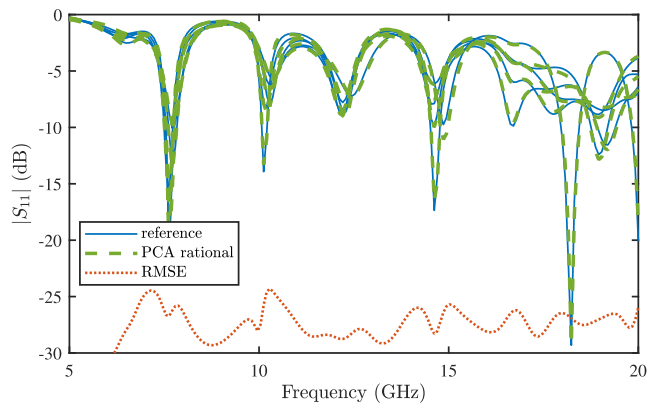
FIGURE 15. Reflection loss of the patch antenna. Curve identification is as in Fig. 13.

FIGURE 17. S-parameters of the PCB interconnect with slotted ground plane. Solid blue lines: reference responses from the CST simulation; dashed green lines: predictions of the PCA-compressed rational model.

D. PCB INTERCONNECT WITH SLOTTED GROUND PLANE

The last example concerns the PCB interconnect with slotted ground plane considered in [38] and shown in Fig. 16. A copper microstrip line with width $t = 0.12$ mm and a thickness of 35 μm runs over a square dielectric substrate of size $a \times b$, with $a = b = 100$ mm, thickness $h = 0.3$ mm, and relative permittivity $\varepsilon_r = 4.3$. The bottom ground plane has a transversal slot of width $w = 0.12$ mm, with a nominal length L and offset d from the midpoint of 15 mm each. These two parameters are considered as independent Gaussian random variables with a 10% relative standard deviation.
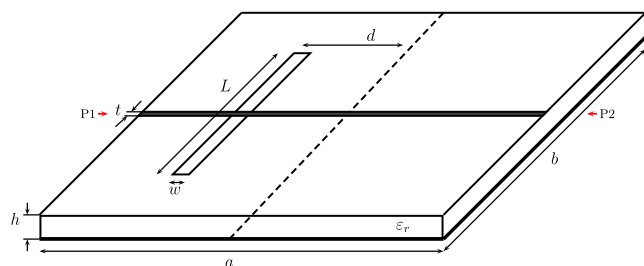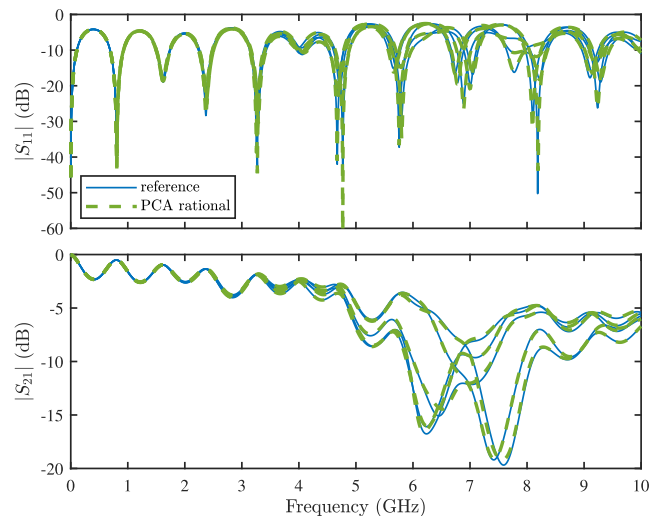

FIGURE 16. PCB interconnect with slotted ground plane [38].

S-parameter samples are computed with Dassault Systèmes Simulia CST Studio Suite from dc to 10 GHz for 1000 random configurations of the uncertain parameters, drawn according to a Latin hypercube design. A rational model with Hermite basis functions of order $p = 4$ is trained using the samples that lie the closest to the first $K = 50$ points of the normally-distributed bivariate Sobol sequence, whereas the rest of the samples is used for validation. Using a PCA truncation threshold of $\epsilon = 10^{-3}$ leads to retaining $\bar{n} = 27$ principal components, making it unfeasible to train a rational model of matching order.

Figure 17 compares a selection of five validation S-parameter samples from the CST simulation (solid blue lines) to the predictions obtained with the PCA-compressed rational model (dashed green lines). An excellent agreement is once again established, despite the large variability of the

response, occurring especially at frequencies above 5 GHz. For this example, the average and maximum RMSE over frequency and port are 2.4394×10^{-2} and 7.3570×10^{-2}, respectively. The training of the model requires 0.2 s.

Furthermore, Fig. 18 shows the PDF of the S-parameters computed at 7 GHz, i.e., the location of the large resonance exhibited by the insertion loss. The proposed method achieves a high accuracy, while requiring a very limited training time.
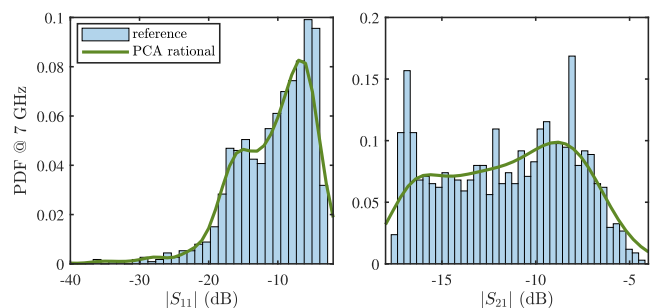

FIGURE 18. PDF of the S-parameters at the frequency of 7 GHz. Histogram: distribution of the reference samples; line: prediction obtained with the PCA-compressed rational model.

VI. CONCLUSION

This paper presented an effective method for constructing rational surrogate models for the uncertainty quantification of linear and passive electrical circuits and electromagnetic structures in the FD, possibly characterized by large datasets in terms of frequency points and number of ports. Rather than training a separate surrogate model for each frequency point and port variable of interest, the data is first compressed using PCA, and a rational model is trained for the principal components only. PCEs are leveraged for the numerator and denominator of the principal components.

Several theoretical insights were provided. First of all, it was demonstrated that setting a relative truncation threshold for the PCA, based on the magnitude of the singular values of the dataset matrix, allows for a rigorous control of the compression accuracy. Second, it was shown that using a rational model for the principal components, in place of the standard single PCE, yields a much better accuracy, in analogy with what was already observed for the direct application of rational models to FD data. Moreover, numerical results show that a model with an expansion order matching the number of principal components yields the best accuracy, although this is not always feasible as it potentially leads to a model of intractable size. Nevertheless, very good accuracy is also attained with lower expansion orders. Finally, it was observed that the PCA-compressed modeling often achieves a lower maximum error over frequency compared to the FD modeling, thanks to the intrinsic regularization properties of the PCA.

The technique was successfully validated based on several application examples, ranging from a simple analytical test case to distributed circuits and electromagnetic structures, for which excellent accuracy was established. Compared to the direct FD modeling, the advocated method requires a much lower training time, in the order of a few seconds instead of several minutes. However, the method is currently limited to a small number of random variables, and it was tested up to three uncertain parameters. Plans for future work include addressing the scalability in terms of number of uncertain parameters, possibly through the use of kernel-based expansions and/or sparse regressions, as well as a more in-depth investigation of the PCA performance.

ACKNOWLEDGMENT

REFERENCES

[1] D. Xiu and G. E. Karniadakis, "The Wiener–Askey polynomial chaos for stochastic differential equations," *SIAM J. Sci. Comput.*, vol. 24, no. 2, pp. 619–622, 2002.

[2] A. Kaintura, T. Dhaene, and D. Spina, "Review of polynomial chaos-based methods for uncertainty quantification in modern integrated circuits," *Electronics*, vol. 7, no. 3, p. 30, Feb. 2018.

[3] S. Vrudhula, J. M. Wang, and P. Ghanta, "Hermite polynomial based interconnect analysis in the presence of process variations," *IEEE Trans. Comput.-Aided Design Integr. Circuits Syst.*, vol. 25, no. 10, pp. 2001–2011, Oct. 2006.

[4] N. Mi, S. X.-D. Tan, Y. Cai, and X. Hong, "Fast variational analysis of on-chip power grids by stochastic extended Krylov subspace method," *IEEE Trans. Comput.-Aided Design Integr. Circuits Syst.*, vol. 27, no. 11, pp. 1996–2006, Nov. 2008.

[5] Z. Zhang, T. A. El-Moselhy, I. M. Elfadel, and L. Daniel, "Stochastic testing method for transistor-level uncertainty quantification based on generalized polynomial chaos," *IEEE Trans. Comput.-Aided Design Integr. Circuits Syst.*, vol. 32, no. 10, pp. 1533–1545, Oct. 2013.

[6] M. R. Rufuie, E. Gad, M. Nakhla, and R. Achar, "Generalized Hermite polynomial chaos for variability analysis of macromodels embedded in nonlinear circuits," *IEEE Trans. Compon., Packag., Manuf. Technol.*, vol. 4, no. 4, pp. 673–684, Apr. 2014.

[7] P. Manfredi, D. V. Ginste, D. De Zutter, and F. G. Canavero, "Stochastic modeling of nonlinear circuits via SPICE-compatible spectral equivalents," *IEEE Trans. Circuits Syst. I, Reg. Papers*, vol. 61, no. 7, pp. 2057–2065, Jul. 2014.

[8] P. Manfredi, R. Trinchero, and D. V. Ginste, "A perturbative stochastic Galerkin method for the uncertainty quantification of linear circuits," *IEEE Trans. Circuits Syst. I, Reg. Papers*, vol. 67, no. 9, pp. 2993–3006, Sep. 2020.

[9] Z. Zhang, X. Yang, I. V. Oseledets, G. E. Karniadakis, and L. Daniel, "Enabling high-dimensional hierarchical uncertainty quantification by ANOVA and tensor-train decomposition," *IEEE Trans. Comput.-Aided Design Integr. Circuits Syst.*, vol. 34, no. 1, pp. 63–76, Jan. 2015.

[10] M. Ahadi and S. Roy, "Sparse linear regression (SPLINER) approach for efficient multidimensional uncertainty quantification of high-speed circuits," *IEEE Trans. Comput.-Aided Design Integr. Circuits Syst.*, vol. 35, no. 10, pp. 1640–1652, Oct. 2016.

[11] Z. Zhang, T.-W. Weng, and L. Daniel, "Big-data tensor recovery for high-dimensional uncertainty quantification of process variations," *IEEE Trans. Compon., Packag., Manuf. Technol.*, vol. 7, no. 5, pp. 687–697, May 2017.

[12] A. K. Prasad and S. Roy, "Accurate reduced dimensional polynomial chaos for efficient uncertainty quantification of microwave/RF networks," *IEEE Trans. Microw. Theory Tech.*, vol. 65, no. 10, pp. 3697–3708, Oct. 2017.

[13] M. Larbi, I. S. Stievano, F. G. Canavero, and P. Besnier, "Variability impact of many design parameters: The case of a realistic electronic link," *IEEE Trans. Electromagn. Compat.*, vol. 60, no. 1, pp. 34–41, Feb. 2018.

[14] R. Trinchero, M. Larbi, H. Torun, F. G. Canavero, and M. Swaminathan, "Machine learning and uncertainty quantification for surrogate models of integrated devices with a large number of parameters," *IEEE Access*, vol. 7, pp. 4056–4066, 2019.

[15] M. A. Dolatsara, J. A. Hejase, W. D. Becker, and M. Swaminathan, "A hybrid methodology for jitter and eye estimation in high-speed serial channels using polynomial chaos surrogate models," *IEEE Access*, vol. 7, pp. 53629–53640, 2019.

[16] M. E. Duman and O. Suvak, "Uncertainty quantification of CMOS active filter circuits: A non-intrusive computational approach based on generalized polynomial chaos," *IEEE Access*, vol. 8, pp. 189246–189261, 2020.

[17] C. Cui and Z. Zhang, "High-dimensional uncertainty quantification of electronic and photonic IC with non-Gaussian correlated process variations," *IEEE Trans. Comput.-Aided Design Integr. Circuits Syst.*, vol. 39, no. 8, pp. 1649–1661, Aug. 2020.

[18] T. Chantrasmi, A. Doostan, and G. Iaccarino, "Padé–Legendre approximants for uncertainty analysis with discontinuous response surfaces," *J. Comput. Phys.*, vol. 228, no. 19, pp. 7159–7180, Oct. 2009.

[19] E. Jacquelin, O. Dessombz, J.-J. Sinou, S. Adhikari, and M. I. Friswell, "Polynomial chaos-based extended Padé expansion in structural dynamics," *Int. J. Numer. Methods Eng.*, vol. 111, no. 12, pp. 1170–1191, Sep. 2017.

[20] M. Rossi, S. Agneessens, H. Rogier, and D. V. Ginste, "Stochastic analysis of the impact of substrate compression on the performance of textile antennas," *IEEE Trans. Antennas Propag.*, vol. 64, no. 6, pp. 2507–2512, Jun. 2016.

[21] P. Manfredi and S. Grivet-Talocia, "Rational polynomial chaos expansions for the stochastic macromodeling of network responses," *IEEE Trans. Circuits Syst. I, Reg. Papers*, vol. 67, no. 1, pp. 225–234, Jan. 2020.

[22] P. Manfredi and S. Grivet-Talocia, "On the exactness of rational polynomial chaos formulation for the uncertainty quantification of linear circuits in the frequency domain," in *Scientific Computing in Electrical Engineering*. New York, NY, USA: Springer, 2020.

[23] V. Yaghoubi, S. Marelli, B. Sudret, and T. Abrahamsson, "Sparse polynomial chaos expansions of frequency response functions using stochastic frequency transformation," *Probab. Eng. Mech.*, vol. 48, pp. 39–58, Apr. 2017.

[24] P. Manfredi and R. Trinchero, "A data compression strategy for the efficient uncertainty quantification of time-domain circuit responses," *IEEE Access*, vol. 8, pp. 92019–92027, 2020.

[25] D. Spina, F. Ferranti, T. Dhaene, L. Knockaert, and G. Antonini, "Polynomial chaos-based macromodeling of multiport systems using an input-output approach," *Int. J. Numer. Model., Electron. Netw., Devices Fields*, vol. 28, no. 5, pp. 562–581, Sep. 2015.

[26] A. J. Laub, *Matrix Analysis for Scientists and Engineers*. Philadelphia, PA, USA: SIAM, 2004.

[27] C. K. Sanathanan and J. Koerner, "Transfer function synthesis as a ratio of two complex polynomials," *IEEE Trans. Autom. Control*, vol. AC-8, no. 1, pp. 56–58, Jan. 1963.

[28] G. H. Golub and C. F. Van Loan, *Matrix Computations*, 4th ed. Baltimore, MD, USA: The Johns Hopkins Univ. Press, 2013.

[29] G. Blatman and B. Sudret, "Adaptive sparse polynomial chaos expansion based on least angle regression," *J. Comput. Phys.*, vol. 230, no. 6, pp. 2345–2367, Mar. 2011.

[30] A. Singhee and R. A. Rutenbar, "Why quasi-Monte Carlo is better than Monte Carlo or Latin hypercube sampling for statistical circuit analysis," *IEEE Trans. Comput.-Aided Design Integr. Circuits Syst.*, vol. 29, no. 11, pp. 1763–1776, Nov. 2010.

[31] I. M. Sobol, "The distribution of points in a cube and the approximate evaluation of integrals," *Zhurnal Vychislitel'noi Matematiki i Matematicheskoi Fiziki*, vol. 7, no. 4, pp. 784–802, 1967.

[32] J. H. Halton, "On the efficiency of certain quasi-random sequences of points in evaluating multi-dimensional integrals," *Numerische Math.*, vol. 2, no. 1, pp. 84–90, 1960.

[33] L. Devroye, *Non-Uniform Random Variate Generation*. New York, NY, USA: Springer-Verlag, 1986.

[34] G. E. P. Box and M. E. Muller, "A note on the generation of random normal deviates," *Ann. Math. Statist.*, vol. 29, no. 2, pp. 610–611, Jun. 1958.

[35] U. von Luxburg and B. Schölkopf, "Statistical learning theory: Models, concepts, and results," in *Handbook of the History of Logic*, vol. 10, D. M. Gabbay, S. Hartmann, and J. Woods, Eds. Amsterdam, The Netherlands: Elsevier, 2011, pp. 651–706.

[36] E. Fevola, A. Zanco, S. Grivet-Talocia, T. Bradde, and M. De Stefano, "An adaptive sampling process for automated multivariate macromodeling based on Hamiltonian-based passivity metrics," *IEEE Trans. Compon., Packag., Manuf. Technol.*, vol. 9, no. 9, pp. 1698–1711, Sep. 2019.

[37] E. Fevola, A. Zanco, S. Grivet-Talocia, T. Bradde, and M. de Stefano, "A 3D passivity-based adaptive algorithm for automated parameterized macromodeling of electromagnetic structures," in *Proc. Int. Conf. Electromagn. Adv. Appl.*, Granada, Spain, Sep. 2019, pp. 22–25.

[38] S. Grivet-Talocia and R. Trinchero, "Behavioral, parameterized, and broadband modeling of wired interconnects with internal discontinuities," *IEEE Trans. Electromagn. Compat.*, vol. 60, no. 1, pp. 77–85, Feb. 2018.

STEFANO GRIVET-TALOCIA (Fellow, IEEE) received the Laurea and Ph.D. degrees in electronic engineering from the Politecnico di Torino, Turin, Italy.

From 1994 to 1996, he was with the NASA/Goddard Space Flight Center, Greenbelt, MD, USA. He co-founded the academic spinoff company IdemWorks, in 2007, serving as the President until its acquisition by CST, in 2016. He is currently a Full Professor of electrical engineering with the Politecnico di Torino. He has authored over 150 journal articles and conference papers. His current research interests include passive macromodeling of lumped and distributed interconnect structures, model-order reduction, modeling and simulation of fields, circuits, and their interaction, wavelets, time-frequency transforms, and their applications.

Dr. Grivet-Talocia was a co-recipient of the 2007 Best Paper Award of the IEEE Transactions on Advanced Packaging. He received the IBM Shared University Research Award, in 2007, 2008, and 2009. He was the General Chair of the 20th and 21st IEEE Workshops on Signal and Power Integrity (SPI2016 and SPI2017). He was an Associate Editor of the IEEE Transactions on Electromagnetic Compatibility, from 1999 to 2001, and is currently serving as an Associate Editor for the IEEE Transactions on Components, Packaging and Manufacturing Technology.

• • •

PAOLO MANFREDI (Senior Member, IEEE) received the M.Sc. degree in electronic engineering from the Politecnico di Torino, Torino, Italy, in 2009, and the Ph.D. degree in information and communication technology from the Scuola Interpolitecnica di Dottorato, Politecnico di Torino, in 2013.

From 2014 to 2017, he was a Postdoctoral Research Fellow with the Research Foundation–Flanders (FWO) of the Electromagnetics Group, Department of Information Technology, Ghent University, Ghent, Belgium. He is currently an Associate Professor with the EMC Group, Department of Electronics and Telecommunications, Politecnico di Torino. His research interests include the several aspects of circuit and interconnect modeling and simulation, including uncertainty quantification, surrogate modeling, signal integrity, and electromagnetic compatibility.

Dr. Manfredi was a recipient of the Outstanding Young Scientist Award at the 2018 Joint IEEE International Symposium on Electromagnetic Compatibility & Asia-Pacific Symposium on Electromagnetic Compatibility, the Best Paper Award at the 2016 IEEE Electrical Design of Advanced Packaging and Systems Symposium, the Best Oral Paper Award and the Best Student Paper Award at the 22nd and 19th IEEE Conference on Electrical Performance of Electronic Packaging and Systems, respectively, the Young Scientist Award at the XXX International Union of Radio Science General Assembly and Scientific Symposium, and the Honorable Mention at the 2011 IEEE Microwave Theory and Techniques Society International Microwave Symposium.